

## Supramolecular Complexes Formed by the Association of Poly(ethyleneimine) (PEI), Sodium Cholate (NaC) and Sodium Dodecyl Sulfate (SDS)

Arlindo C. Felipe,<sup>\*a</sup> Ismael C. Bellettini,<sup>a</sup> Renato Eising,<sup>a</sup> Edson Minatti<sup>a</sup> and Fernando C. Giacomelli<sup>b</sup>

<sup>a</sup>Departamento de Química, Universidade Federal de Santa Catarina, 88040-900 Florianópolis-SC, Brazil

<sup>b</sup>Centro de Ciências Naturais e Humanas, Universidade Federal do ABC, 09210-170 Santo André-SP, Brazil

A formação de complexos supramoleculares em solução aquosa pela associação do polieletrólito poli(etilenoimina) (PEI) com misturas do biossurfactante colato de sódio (NaC) e o surfactante aniônico dodecil sulfato de sódio (SDS) foi aqui investigado usando as técnicas de condutivimetria, tensiometria, fluorimetria, espalhamento de raios X a baixos ângulos (SAXS) e medidas de pH. Os resultados de fluorimetria, condutivimetria e medidas de pH levaram à conclusão de que os monômeros de NaC e SDS ligam-se primeiramente em sítios específicos das cadeias do polieletrólito PEI via interação eletrostática e posteriormente através de associação cooperativa. A interação do NaC com o PEI é mais fraca do que a interação do SDS com o PEI, porém, a adição de SDS ao sistema NaC-PEI levou à formação de micelas mistas SDS-NaC que interagiram fortemente com o polieletrólito PEI. Os resultados de SAXS sugeriram que o complexo supramolecular possui característica elipsoidal e essa forma não depende da concentração de surfactante nem da  $\chi_{\text{NaC}}$ .

The formation of supramolecular complexes produced by association of poly(ethyleneimine) (PEI) and mixtures of sodium cholate (NaC) and sodium dodecyl sulfate (SDS) was investigated by pH, electrical conductivity, fluorescence spectroscopy and small angle X-ray scattering (SAXS) measurements. The fluorescence linked to previously measured values of pH and conductivity led to the conclusion that NaC and SDS molecules firstly bind to specific sites of the PEI chains via electrostatic interaction and secondly undergo self-assembly through regular cooperative association. The interaction of NaC with the polyelectrolyte PEI is weaker than that of SDS and the addition of SDS to the NaC-PEI system led to the formation of mixed NaC-SDS micelles which stronger interact with PEI. The SAXS results suggested that the micellar aggregates have a considerably ellipsoidal characteristic and the micellar shape is not affected by the surfactant concentration nor by  $\chi_{\text{NaC}}$ .

**Keywords:** sodium cholate, sodium dodecyl sulfate, poly(ethyleneimine), polymer-surfactants interaction

### Introduction

Bile salts are naturally-occurring amphiphilic molecules. They are physiologically important in the solubilization and transport of fats and lipids. The structure of bile salts in water has been extensively investigated. Although they are comparable to common surfactants, the general conclusion is that biosurfactants self-assemble in a different way than the standard surfactants.<sup>1-13</sup>

Poly(ethyleneimine) (PEI) is a member of a large family of water-soluble polyamines having different molecular weights ( $M_w$ ) and polymer architectures. Polyamines are weak bases and exhibit a cationic character depending on the degree of protonation. PEI has been extensively studied (particularly the branched form) due to its intense use in the formulation of drugs, thickeners, flocculating agents, personal care products, food products, detergents and adhesives. It has also been used for biological purposes to purify soluble proteins and flocculate cellular contaminants, such as nucleic acids and lipids. Furthermore, PEI has been established as a valuable tool in biotechnological

\*e-mail: arlindofelippe@hotmail.com

<sup>#</sup>Present address: Universidade Federal da Fronteira Sul (UFFS), 89813-140 Chapecó-SC, Brasil - <http://www.uffs.edu.br>

formulations for transfection and expression of genes *in vitro* and *in vivo*<sup>14,15</sup> and also in catalysis as an artificial enzyme.<sup>16</sup>

Polymers and surfactants associate in aqueous solution leading to the formation of thermodynamically stable complexes and the final physicochemical characteristics differ from those observed in pure surfactant micellar solutions.<sup>17-19</sup> The mixture induces, for example, the formation of aggregates at an early stage than the critical micelle concentration (*cmc*) of the pure surfactant in solution in a point that it is called critical aggregation concentration (*cac*). Therefore, it is possible to prepare formulations by adding a polymeric component to a surfactant solution with a reduced amount of the latter one having the same or improved properties than the formulations containing solely surfactants.<sup>17,19</sup>

Our research group has extensively studied micellar systems formed by the self-assembly of copolymers<sup>20,21</sup> and surfactants.<sup>22-25</sup> We have investigated a large collection of synthetic polymers and biopolymers,<sup>26-28</sup> as well as surfactants and biosurfactants.<sup>27-30</sup> Interestingly, interactions between water-soluble uncharged polymers and the anionic surfactants have been widely investigated for several decades. On the other hand, few studies concerning the interactions of mixtures of bile salts and polyelectrolytes are found in the literature.

Polyelectrolytes, such as PEI, can interact with specific surfactants leading to the formation of polymer-surfactant complexes. The structure of such complexes is dependent on the way in which the interaction occurs. These interactions might be purely through electrostatic interactions or influenced by the molecular characteristics of the charged groups, the flexibility and architecture of the polymer chains and the types of counter-ions present in the system.<sup>31</sup> Some researchers suggest that the formation of a polyelectrolyte-surfactant complex is accompanied by conformational changes in the polymer chains. Several techniques have been used to monitor these structural changes including fluorescence, light scattering, small angle X-ray scattering (SAXS) and viscosity. Recently, SDS-PEI complexes have been investigated.<sup>31-36</sup> Wang *et al.*<sup>32</sup> explored the influence of the pH on the binding properties of SDS in linear and branched PEI. Winnik *et al.*<sup>31,33,34</sup> studied the influence of the pH values and surfactant concentration on the SDS-PEI interaction through conductimetry, light scattering, nuclear magnetic resonance (NMR), microcalorimetry and electrical conductivity. Meszaros *et al.*<sup>35</sup> also studied this system and demonstrated that the interaction occurs in two steps: firstly there is a specific binding of dodecyl sulfate ions (in the monomer form) to protonated amine

groups (evidenced by the increase in pH) and, secondly, a cooperative interaction of a hydrophobic nature occurs. Bastardo *et al.*<sup>36</sup> performed light scattering and small angle neutron scattering measurements on SDS/PEI complexes in order to probe the structure of the complexes at different pH values and SDS concentration. The experiments evidenced the presence of disk-like aggregates at low SDS concentration and more complex three-dimensional structures with increasing surfactant concentration.

Herein, we focus on the association of the bile salt sodium cholate (NaC) and mixtures of NaC and SDS and the polyelectrolyte poly(ethyleneimine) (PEI). The main aim was to verify and discuss the variations in the parameters such as critical micelle concentration (*cmc*), critical aggregate concentration (*cac*) and polymer saturation point (*psp*) as a function of surfactant concentration and molar fraction of the biosurfactant ( $\chi_{\text{NaC}}$ ) in the presence of PEI, as well as in PEI-free solutions. The investigations were supported by pH value, electrical conductivity, steady-state fluorescence of pyrene and SAXS measurements. In this regard, a model of the interaction between SDS, NaC and their mixtures with the polyelectrolyte PEI is proposed.

## Experimental

### Materials

Sodium dodecyl sulfate (SDS), sodium cholate (NaC) and pyrene were supplied by Sigma and used without further purification. Poly(ethyleneimine) (PEI),  $M_w = 25000 \text{ g mol}^{-1}$  was purchased from Aldrich. A stock PEI solution was prepared by dissolving the polymer in pure distilled water and the resulting solution was stirred gently at room temperature overnight. This stock solution was used to prepare those containing the surfactants. The PEI concentration is given as mass/volume percentage (% m/v) and the surfactant concentration  $\text{mmol L}^{-1}$ . All results were obtained at  $(25.0 \pm 0.1) \text{ }^\circ\text{C}$ .

### pH and specific conductivity measurements

The pH value and specific conductivity measurements were performed in the following way: small amounts of aqueous stock solutions of surfactants were added to a known volume of water in a dilution cell. After each addition of stock solution, the pH value and the specific conductivity were measured by the immersed pH and conductivity electrodes. The resulting concentration after each addition was corrected considering the total volume of the cell. Electrical conductivity data were acquired by means of a water-jacketed flow dilution cell using a 170 ATTORION

conductometer. The pH value measurements were acquired in a similar way using a Beckman  $\phi$  71 pH meter with a combined glass electrode. The aliquots were added using a semi-automatic burette Metrohm Herisau (Multi-Burette type model E-485).

#### *Steady-state fluorescence*

Measurements of the steady-state fluorescence of pyrene were performed in water. Firstly, a stock pyrene (Aldrich 99%) solution ( $0.001 \text{ mol L}^{-1}$ ) was prepared in dry ethanol and a  $10^{-6} \text{ mol L}^{-1}$  pyrene aqueous solution was then prepared by adding  $0.25 \text{ mL}$  of the stock solution to  $250 \text{ mL}$  of water. The surfactant and surfactant-PEI samples were prepared using the aqueous pyrene solution. A steady-state fluorescence spectrum of pyrene was recorded on a Hitachi F4500 Spectrofluorimeter equipped with a thermostated cell holder set at  $25.0 \text{ }^\circ\text{C}$  and the samples were continuously stirred in a quartz cell with a path length of  $10 \text{ mm}$ . Both the slits of excitation and emission monochromators were adjusted to  $2.5 \text{ nm}$ . The samples were excited at  $336 \text{ nm}$  and the emission spectra were recorded from  $360$  to  $500 \text{ nm}$ . Typically, the fluorescence spectrum was recorded after the addition of each  $\mu\text{L}$  of surfactant solution. The  $I_1/I_3$  ratio was estimated by taking into account the ratio of the maximum peak intensity at  $372.8 \text{ nm}$  ( $I_1$ ) and at  $384.0 \text{ nm}$  ( $I_3$ ).<sup>37-41</sup>

#### *Small angle X-ray scattering (SAXS)*

The SAXS experiments were performed at the SAXS2 beamline of the Brazilian Synchrotron Light Laboratory (LNLS, Campinas-SP, Brazil). The wavelength ( $\lambda$ ) of the incoming beam was set to  $0.1488 \text{ nm}$ . The samples were injected into a  $1 \text{ mm}$ -thick sample holder specially designed for the LNLS SAXS beamlines.<sup>42</sup> The collimated beam crossed the samples through an evacuated flight tube ( $P < 0.1 \text{ mBar}$ ) and was scattered to a 2D CCD marCCD detector with active area of  $16 \text{ cm}^2$ . The sample-to-detector distance was set to  $809 \text{ mm}$  (Silver Behenate was used as the sample-to-detector distance calibration since it has a well-known lamellar structure,  $d = 58.48 \text{ \AA}$ ). In this geometry, the  $q$  range was covered from  $0.18$  to  $4.5 \text{ nm}^{-1}$ . In all cases, the 2D-images were found to be isotropic and were corrected by taking into account the detector dark noise and normalized by the sample transmission. The corrected and normalized 2D images of the samples were subtracted from the corrected and normalized 2D image of the solvent, and the resulting images were then azimuthally integrated considering the  $360^\circ$  scan to give the final  $I$  vs.  $q$  profiles. The above procedures were carried out using the FIT2D software developed by Hammersley.<sup>43</sup> The scattering

profiles of the aggregates were modelled by considering the form factor  $P(q)$  of an ellipsoidal core-shell object with the inner core and the outer shell having different scattering length densities. The interparticle structure factor  $S(q)$  was taken into account by using the mean spherical approximation (MSA) according to Hayter and Penfold.<sup>44</sup> A more detailed description of the model used is given in the next section. The fitting procedures were performed using the SASfit software which uses the least-squares fitting approach consisting of minimizing the squared chi ( $\chi^2$ ). The SASfit software package was developed by Kohlbrecher and is available online.<sup>45</sup>

## Results and Discussion

#### *pH and specific conductivity measurements*

The aggregation processes were firstly monitored by means of conductivity and pH titration of the polymer solutions with surfactant solutions. These techniques provide useful information on the ionic mobility and availability of free ions in the system. By means of conductivity measurements, it is possible to observe the onset of surfactant aggregation in the polymer chains as well as the polymer saturation through the surfactant.<sup>46-49</sup> In the titration process for strong polyelectrolyte case, the electrical conductivity variation is proportional to the amount of added surfactant, whereas for weak polyelectrolytes, such as PEI, it is dependent on the dissociation equilibria that are related to the degree of ionization of the polymer chain.

The variations of the specific conductivity and pH value during the titration of a PEI solution  $0.2\% \text{ m/v}$  with known amounts of SDS and NaC are given in Figures 1A and 2A, respectively. Figures 1B and 2B show the specific conductivity and pH profiles at the beginning of each titration procedure.

Three different regions can be quite clearly distinguished in the specific conductivity and pH profiles given in Figures 1 and 2.

#### *Surfactant concentration below $c_{ac}$*

The pH value of a  $0.2\% \text{ m/v}$  PEI aqueous solution is alkaline (pH *ca.* 9.5) due to the presence of the protonated amine groups in the polymer chains (equation 1). The pH value quickly increases from 9.5 to 10.0 with the addition of SDS up to *ca.*  $1.0 \text{ mmol L}^{-1}$  (Figure 1) and from 9.5 to 9.9 with the addition of NaC up to *ca.*  $5.0 \text{ mmol L}^{-1}$  (Figure 2). The addition of small amounts of an anionic surfactant (whether SDS or NaC) promotes the stabilization of the weak acid conjugate ( $\text{R}_3\text{NH}^+$ ), thus increasing the pH value

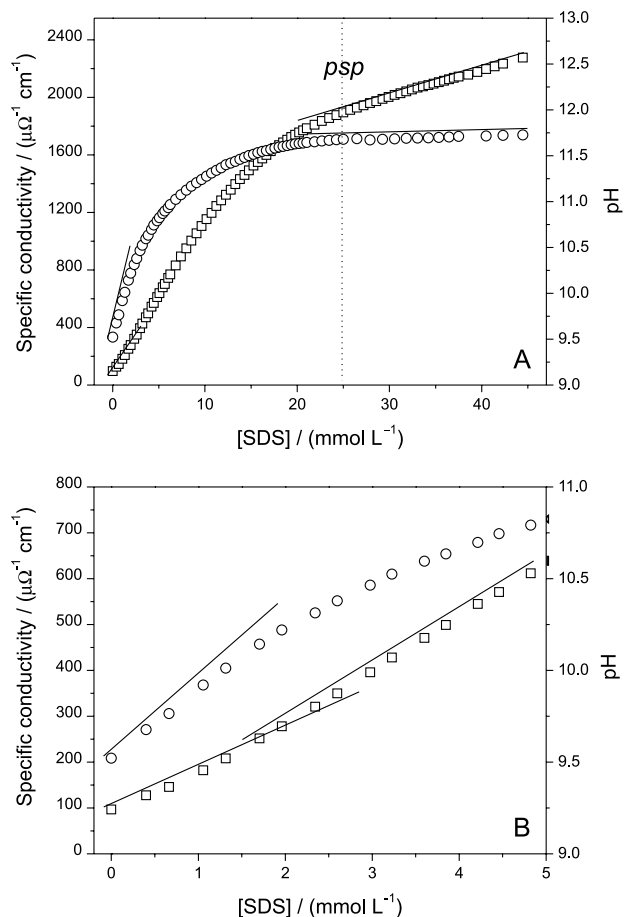


**Figure 1.** Specific conductivity (□) and pH (○) variation during the titration of PEI solution 0.2% m/v with SDS (A). The profiles at the beginning of the titrations are enlarged in (B). The drawn lines are just eye-guides.

of the solution. The specific binding of dodecyl sulfate (DS<sup>-</sup>) or cholate anions to the positively charged sites of the PEI chains shifts the acid-base equilibrium towards the right-hand side of equation 1, *i.e.*, in the direction of hydroxide formation.



In the same region, the increase in the solution electrical conductivity is related to the higher equivalent conductance of the hydroxyl (198.6 Ω<sup>-1</sup> cm<sup>2</sup> mol<sup>-1</sup>) compared to the dodecyl sulfate (21.59 Ω<sup>-1</sup> cm<sup>2</sup> mol<sup>-1</sup>) or cholate (13.90 Ω<sup>-1</sup> cm<sup>2</sup> mol<sup>-1</sup>) ion.<sup>29</sup> At the end of the binding process, *i.e.*, when all the positively charged sites of PEI are filled, the polymer chains behave as a neutral entity and the interaction with the surfactants SDS and NaC starts to take place through a cooperative process similar to the system constituted by the surfactant SDS and the neutral polymer poly(ethylene oxide) that is widely discussed in the literature.<sup>18,22,29,50,51</sup> The beginning of the cooperative association between

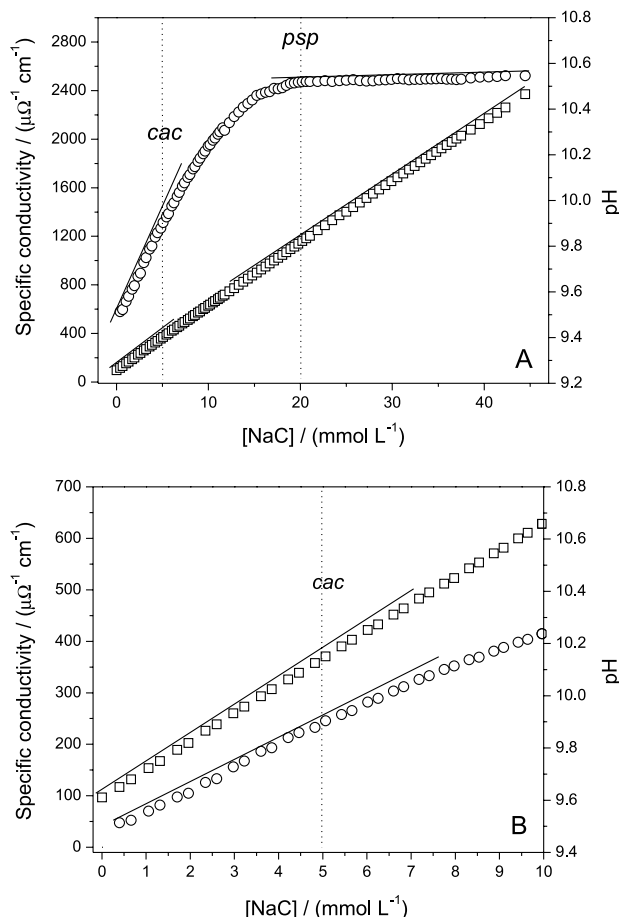


**Figure 2.** Specific conductivity (□) and pH (○) variation during the titration of a PEI solution 0.2% m/v with NaC (A). The profiles at the beginning of the titrations are enlarged in (B). The drawn lines are just eye-guides.

polymer and surfactants, defined here as *cac*, starts at the first discontinuity in the profiles of specific conductivity *vs.* surfactant concentration, at *ca.* 5.0 mmol L<sup>-1</sup> for NaC. For the PEI-SDS system, the profile does not show clearly the *cac*, meaning that such technique is limited in the determination surfactant under low concentrations. Figures 1B and 2B show in details the regions.

#### Surfactant concentration between *cac* and *psp*

Moving from the *cac* to a higher surfactant concentration, the pH value of the solution increases less abruptly than at the beginning of the titrations. This occurs up to around 25.0 mmol L<sup>-1</sup> when the pH value is approximately 11.7 for the SDS system (Figure 1A) whereas the same phenomenon is observed up to 20.0 mmol L<sup>-1</sup>, when the pH value of the solution is *ca.* 10.5 for the NaC system (Figure 2A). These concentrations indicate the second point of discontinuity in the profiles of specific conductivity *vs.* surfactant concentration, which is denoted here as the saturation point of the polymer, *psp*. The formation of polymer-surfactant

supramolecular complexes takes place in the region between *cac* and *psp*.

#### Surfactant concentration above *psp*

Finally, the pH value at quantities above *psp* is surfactant-concentration independent. The pH value remained at *ca.* 11.7 for SDS and at *ca.* 10.5 for NaC. This characterizes the third region of the aggregation profile. This behavior can be attributed to the formation of free micelles of SDS and NaC which are in equilibrium with the SDS-PEI and NaC-PEI supramolecular complexes. Figure 3 schematically represents the common steps of the PEI-surfactant associations.

#### Fluorescence measurements

Techniques using fluorescent probes such as pyrene have been extensively used to monitor the surfactant aggregation processes.<sup>5,33,37,38,40,41</sup> They are undoubtedly useful in determining key parameters, such as *cmc* and *cac*. The fluorescent probe pyrene has five fluorescent bands and the ratio between its  $I_1$  (372.8 nm) and  $I_3$  (384.0 nm) bands is sensitive to small changes in the environmental polarity. It is possible to monitor pyrene migration from a polar (water) to an apolar (micellar core) environment through the fluorescence spectroscopy by measuring the  $I_1/I_3$  ratio.<sup>40,41</sup> The  $I_1/I_3$  ratio of pyrene is used as a criterion to evaluate the micropolarity of the microenvironments of micellar aggregates, and extreme values of this polarity scale comprise *ca.* 1.8 for water and *ca.* 0.6 for hexane.<sup>40,41</sup> Since the pyrene probe migrates from the polar aqueous medium to the apolar micellar cores during the surfactant micellization, the  $I_1/I_3$  ratio becomes possible to follow the aggregation path.

The profiles of  $I_1/I_3$  ratio *vs.* [SDS] and [NaC] in PEI-free solution and in the presence of 0.2% m/v PEI

are shown in Figures 4A and 4B, respectively. The  $I_1/I_3$  ratio in the presence of small amounts of SDS or NaC is around 1.80-1.85, what is consistent with the water polarity.<sup>5</sup> The *cmc* values were determined in polymer-free solution at the surfactant concentration where the upper plateau ends. According to this methodology, the *cmc* values for SDS and NaC were determined as 7.0 and 10.0 mmol L<sup>-1</sup>, respectively. These *cmc* values are in agreement with the ones found in the literature and were measured through surface tension (6.0 mmol L<sup>-1</sup> for SDS and 10 mmol L<sup>-1</sup> for NaC)<sup>29</sup> and electrical conductivity (7.8 mmol L<sup>-1</sup> for SDS).<sup>30</sup> The presence of PEI in the SDS solution shifts the profile considerably and the upper plateau ends at a remarkably lower SDS concentration (Figure 4A). The SDS-PEI solution shows a clear *cac* at 0.07 mmol L<sup>-1</sup>. Likewise, the addition of PEI to the NaC solution (Figure 4B) led to a shift in the *cac* towards a lower NaC concentration, however, not as low as that one for the SDS system. The *cac* in the latter case is at around 5.0 mmol L<sup>-1</sup>. Hence, the presence of a *cac* in both systems can be used as a fingerprint of the formation of SDS-PEI and NaC-PEI supramolecular complexes developed through a cooperative process.

The determination of a *cac* in the polymer-surfactant mixture presupposes the existence of a driving force similar to that of normal surfactant micellization with strongly cooperative binding. The *cac* value is dependent on the strength of the polymer-surfactant interaction and can be quantitatively evaluated by using the phase separation model of micelle formation: the free energy for the equilibrium of free micelles and micelle-polymer aggregates represents the polymer-surfactant interaction and is given by equation 2.<sup>52</sup>

$$\Delta G^o = RT \ln \left( \frac{cac}{cmc} \right) \quad (2)$$

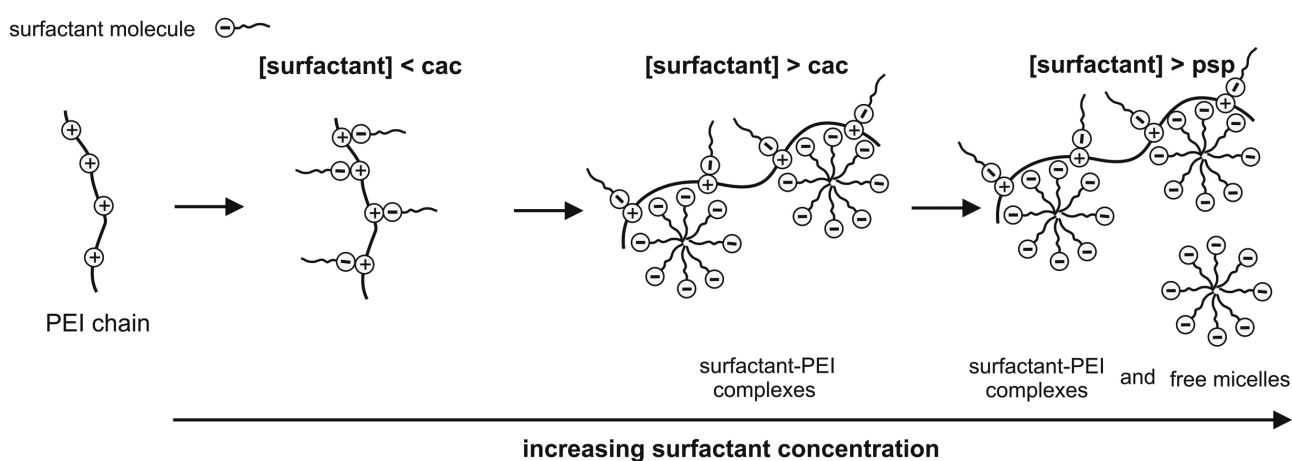


**Figure 3.** The schematic representation of supramolecular complexes.

The pH value, specific conductivity and fluorescence measurements suggest that the bile salt NaC binds to PEI chains less intensely than SDS, since the *cac* is around two

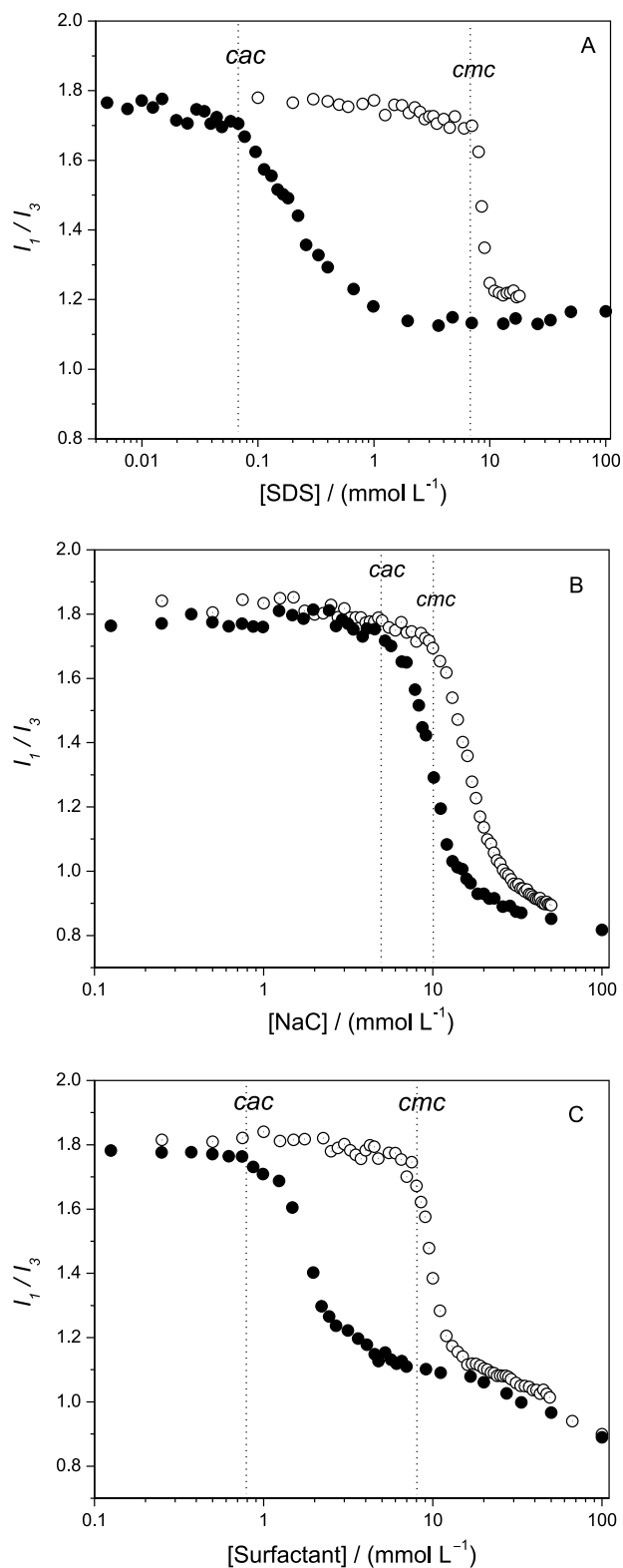


**Figure 4.**  $I_1/I_3$  vs. surfactant concentration in polymer-free (○) or 0.2% m/v PEI (●) solution (A - SDS, B - NaC and C -  $\chi_{\text{NaC}} = 0.90$ ).

orders of magnitude smaller than *cmc* in the latter case, whereas the *cac* is only around half the *cmc* for NaC-PEI. Therefore, the *cac*/*cmc* ratio is smaller in the SDS system and consequently  $\Delta G^\circ$  is more negative. In order to promote the association of the biosurfactant NaC to PEI at lower surfactant concentrations, known amounts of SDS were added into the mixture. The results are shown in Table 1.

**Table 1.** Micellization parameters obtained from the SDS-NaC-PEI mixtures

| $\chi_{\text{NaC}}$ | [ <i>cmc</i> ]/<br>(mmol L <sup>-1</sup> ) | [ <i>cac</i> ]/<br>(mmol L <sup>-1</sup> ) | <i>cac</i> / <i>cmc</i> | $\Delta G^\circ /$<br>(kJ mol <sup>-1</sup> ) |
|---------------------|--|--|-------------------------|---|
| 0.00                | 7.0  | 0.07                                       | 0.010                   | -11.42  |
| 0.10                | 6.5  | 0.10                                       | 0.015                   | -10.35  |
| 0.25                | 6.1  | 0.15                                       | 0.025                   | -9.19   |
| 0.50                | 6.4  | 0.20                                       | 0.031                   | -8.59   |
| 0.75                | 7.9  | 0.25                                       | 0.032                   | -8.56   |
| 0.90                | 8.0  | 0.80                                       | 0.100                   | -5.71   |
| 1.00                | 10.0                                       | 5.00                                       | 0.500                   | -1.72   |

The addition of a small amount of SDS to the NaC-PEI system was sufficient to stabilize the PEI-SDS-NaC supramolecular complexes. At  $\chi_{\text{NaC}} = 0.9$ , the *cac* determined was 0.8 mmol L<sup>-1</sup>, which is well below the *cmc* (8.0 mmol L<sup>-1</sup>) in the polymer-free solution, as can be seen in Figure 4C and Table 1. Furthermore, a gradually decrease in the *cac*/*cmc* parameter can be noted by reducing  $\chi_{\text{NaC}}$ .

It can also be seen that, the interaction between mixed micelles and PEI is relatively weak ( $\Delta G^\circ$  is less negative) for  $\chi_{\text{NaC}} > 0.75$  since the micelles are NaC-rich. The strength of the interaction increases in the intermediate region ( $0.25 \leq \chi_{\text{NaC}} \leq 0.75$ ), as noted by the reduction in *cac*, and there is the clear formation of a plateau in the  $\Delta G^\circ$  vs.  $\chi_{\text{NaC}}$  profile (Figure 5). Finally, the interaction

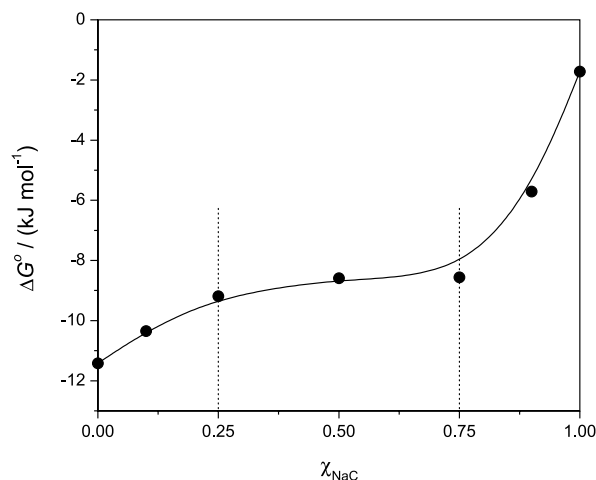


**Figure 5.**  $\Delta G^\circ$  vs.  $\chi_{\text{NaC}}$ . The drawn lines are just eye-guides.

process at  $\chi_{\text{NaC}} < 0.25$  occurs strongly since the mixed micelles are SDS-rich.

#### Small angle X-ray scattering measurements

The SAXS measurements were acquired in the region between (5-20 mmol L<sup>-1</sup>) *cac* and *psp* and at  $0.25 < \chi_{\text{NaC}} < 0.75$ , hence, in the range where only surfactant-PEI complexes and nonexistence of free micellar aggregates were detected by previous pH value, conductimetry and fluorescence measurements.

The SAXS scattering intensity ( $I(q)$ ), of an isotropic solution of monodisperse particles embedded in a matrix with a constant scattering length density is given by:

$$I(q) = NP(q)S(q) \quad (3)$$

wherein  $N$  is in the number of particles *per* unit volume,  $P(q)$  is the form factor of an individual particle and  $S(q)$  is related to the interference particle factor which arises from long-range correlations between scattering centers. The  $P(q)$  form factor of the scattering objects is linked to their size and shape. In this study, the micellar aggregates were geometrically modeled as ellipsoidal core-shell objects with different scattering length densities of the apolar and polar regions. The description of the size and shape of SDS micelles by using an ellipsoidal core-shell model is straightforward<sup>53,54</sup> and it is schematically represented in Figure 6.

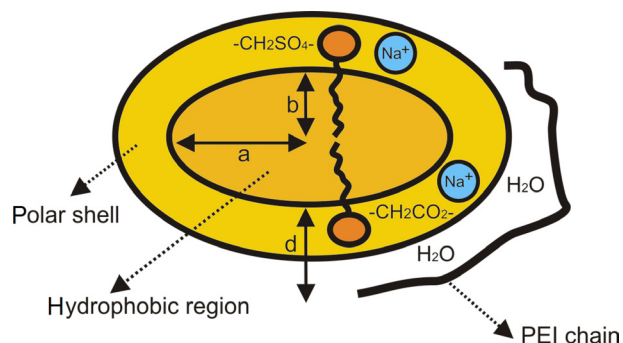


**Figure 6.** Schematic representation of the NaC-SDS-PEI supramolecular complexes.

The aggregates were assumed to be formed of a hydrophobic ellipsoidal region with principal axes  $a$  and  $b$  ( $a > b$ ), which contains the surfactants hydrophobic tail. In the hydrophilic shell of thickness  $d$ , there is the surfactant polar headgroup, the first methylene units,<sup>55</sup> the hydration of water molecules, a fraction of counterions and possibly a fraction of the neutralized PEI chain bounded to the polar region.<sup>56</sup> The scattering length density of the solvent water

( $\rho_{\text{water}}$ ) was a fixed parameter ( $\rho_{\text{water}} = 9.42 \times 10^{-6} \text{ \AA}^{-2}$ ). Besides  $a$ ,  $b$  and  $d$ , the scattering length density of the polar shell ( $\rho_{\text{shell}}$ ) and of the hydrophobic core ( $\rho_{\text{core}}$ ) were fitting parameters of  $P(q)$ .

The  $S(q)$  structure factor was taken into account by using the mean spherical approximation (MSA) developed by Hayter and Penfold.<sup>44</sup> It describes the structure factor of charged objects in a dielectric medium and combined with  $P(q)$  allows the inclusion of interparticle interference effects due to screened Coulomb repulsion between charged particles. The salt concentration used to compute the ionic strength of the solution, which in turn is used to compute the Debye screening length, was fixed as the molar concentration of surfactant monomers. The effective particle charge ( $Z$ ) was a free parameter of  $S(q)$ .

The SAXS measurements were employed in order to evaluate morphological evolutions in the supramolecular complexes as the concentration of surfactants and the molar fraction of NaC ( $\chi_{\text{NaC}}$ ) change. Figure 7 shows representative SAXS patterns measured for  $\chi_{\text{NaC}} = 0.25$ , 0.2% m/v PEI and different concentrations of surfactant according to the legend.

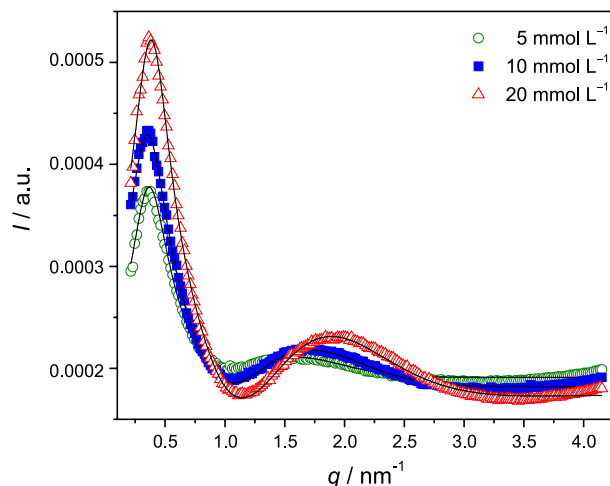


**Figure 7.** SAXS patterns measured for  $\chi_{\text{NaC}} = 0.25$ , 0.2% m/v PEI and different concentrations of surfactant according to the legend.

Visually, the SAXS profiles across the whole concentration range are similar. There is always a broad shoulder at around  $q$  ca. 1.5-2.0 nm<sup>-1</sup> and a pronounced and sharp scattering peak at the low- $q$  region ( $q$  ca. 0.36 nm<sup>-1</sup>). The broad shoulder is related to the intramicellar form factor, whereas the latter feature is a fingerprint of the interference function related to the interaction between scattering centres (charged micelles).<sup>53</sup> Qualitatively, it can be seen that the intensity of the form factor bump increases as the surfactant concentration increases. It also moves towards the long- $q$  region. Furthermore, interparticle

**Table 2.** Micellar parameters directly obtained from SAXS fittings for  $\chi_{\text{NaC}} = 0.25$ , 0.2% m/v PEI and different concentrations of surfactant

| [surfactant] / (mmol L <sup>-1</sup> ) | <i>a</i> / nm | <i>b</i> / nm | <i>d</i> / nm | ( <i>a</i> + <i>d</i> ) / nm | <i>alb</i> | $\rho_{\text{core}} / 10^{-6} \text{ \AA}^{-2}$ | $\rho_{\text{shell}} / 10^{-6} \text{ \AA}^{-2}$ | <i>Z</i> |
|--|---------------|---------------|---------------|------------------------------|------------|---|--|----------|
| 5.0                                    | 2.69          | 1.11          | 1.63          | 4.32                         | 2.4        | 7.77  | 9.66   | 17.4     |
| 10.0                                   | 2.66          | 1.05          | 1.65          | 4.31                         | 2.5        | 7.73  | 9.68   | 17.7     |
| 12.5                                   | 2.58          | 1.04          | 1.51          | 4.09                         | 2.5        | 7.82  | 9.67   | 18.4     |
| 15.0                                   | 2.51          | 1.02          | 1.40          | 3.91                         | 2.4        | 7.70  | 9.69   | 18.8     |
| 20.0                                   | 2.44          | 0.96          | 1.29          | 3.73                         | 2.5        | 7.66  | 9.68   | 19.0     |

interference is always visible and indeed related to the electrostatic repulsion between the negatively charged micelles. It should be noted that although  $I(q)$  is given in arbitrary units (a.u.), the SAXS profiles were normalized by the transmitted X-ray intensity integrated over time and thus they can be quantitatively compared. One may notice that when the surfactant concentration increases, the intensity of the sharp low- $q$  range peak increases. It means that the repulsion forces between close charged objects are enhanced due to the higher effective charge of the micelles (higher concentration of negatively charged entities forming the micellar aggregates). On the other hand, the peak position is not strongly affected by the surfactant concentration and remains very close to  $q$  ca.  $0.36 \text{ nm}^{-1}$ .

The solid black lines in Figure 7 are the fitting results by using  $P(q)$  and  $S(q)$  modelled as detailed above. The fitting approach describes the experimental results reasonably well. The extracted parameters for this set of measurements are summarized in Table 2.

For the particular molar fraction of NaC ( $\chi_{\text{NaC}} = 0.25$ ), the core and shell scattering length densities ( $\rho_{\text{core}}$  and  $\rho_{\text{shell}}$ ) remained essentially the same,  $\rho_{\text{shell}}$  being even higher than  $\rho_{\text{water}}$ , as previously demonstrated for other SDS complexes.<sup>53,54</sup> The  $alb$  ratio gives a qualitative evaluation of the micellar shape and it can be noted that the micellar core has a considerably ellipsoidal characteristic since  $alb$  ca. 2.5. As a matter of comparison, the ellipsoidal characteristic of CTAC micelles interacting with TPPS<sub>4</sub> was found to be even more pronounced with an  $alb$  (axial ratio) ca. 3.0.<sup>57</sup> Regarding the hydrophobic region, the predicted length of a dodecyl chain is ca. 1.67 nm.<sup>58</sup> However, it is hard to evaluate the structural packing of the micellar hydrophobic core since it deals with SDS/NaC mixed micelles. Nevertheless, they are ellipsoids with the smallest semi-axis (ca. 1.0 nm) and the longest semi-axis (ca. 2.5 nm). Therefore, the dimensions are reasonable to accommodate the hydrophobic section of the polymer-surfactant complexes, albeit the structural packing has to be further evaluated.

In the current study, the  $alb$  ratio remained almost the same across the whole range of concentration, meaning that the micellar shape is not affected by the surfactant concentration. Consequently, the changes in

$P(q)$  (Figure 7) must be related to changes in the micellar size. The displacement of the bump towards the long- $q$  region, when the surfactant concentration increases, gives a qualitative indication that the complexes are smaller at higher concentrations, as seen quantitatively in Table 2. A systematic reduction in the dimension ( $a + d$ ) is observed in the range of the investigated concentration.

Since the core scattering length density is higher than the shell scattering length density contrast ( $(\rho_{\text{core}} - \rho_{\text{water}}) > (\rho_{\text{shell}} - \rho_{\text{water}})$ ), the former ( $\rho_{\text{core}} - \rho_{\text{water}}$ ) contributes to a greater extent to the form factor region profile. The increase in the surfactant concentration increases the number of aggregation of the mixed micelles (not shown here). Therefore, a greater contribution of ( $\rho_{\text{core}} - \rho_{\text{water}}$ ) to the form factor region is expected and consequently a more pronounced bump is observed.

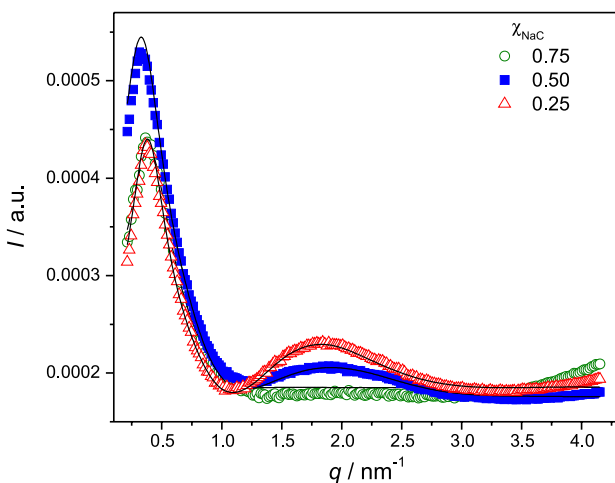
The observed polar thickness ( $d$ ) can be considered to be remarkably large. However, this is not surprising since it probably comprises a series of different entities, as previously described. Finally, the effective surface charge of the micelles ( $Z$ ) is also influenced by the surfactant concentration. As the number of aggregation of the mixed micelles increases, a higher number of negatively charged surfactant headgroups composes the polar region of the complexes. Thus, it is straightforward to conclude that the repulsion between the aggregates will be enhanced, as experimentally evidenced in the intensity of the interference peak, by the increase in the effective surface charge of the aggregates.

Figure 8 shows the representative SAXS patterns obtained for [surfactant] = 15 mmol L<sup>-1</sup>, 0.2% m/v PEI and different  $\chi_{\text{NaC}}$  values. The solid black lines correspond to the best fits obtained using the above-detailed model. The extracted fitting parameters are summarized in Table 3.

The bump in the SAXS profiles is only visible when  $\chi_{\text{NaC}} < 0.75$ . The shape of the supramolecular complexes ( $alb$ ) and the effective surface charge ( $Z$ ) are unaffected by  $\chi_{\text{NaC}}$ . The micellar size is slightly dependent on  $\chi_{\text{NaC}}$ . The micellar growth from  $\chi_{\text{NaC}} = 0.75$  to  $\chi_{\text{NaC}} = 0.25$  is of only 0.17 nm ( $a + d$ ). Qualitatively, a slight (almost negligible) displacement of the form factor bump towards the low- $q$  region is seen in Figure 8. However, its intensity is strongly influenced by  $\chi_{\text{NaC}}$ .

**Table 3.** Micellar parameters directly obtained from SAXS fittings for [surfactant] = 15 mmol L<sup>-1</sup>, 0.2% m/v PEI and different  $\chi_{\text{NaC}}$ 

| $\chi_{\text{NaC}}$ | $a / \text{nm}$ | $b / \text{nm}$ | $d / \text{nm}$ | $(a + d) / \text{nm}$ | $a/b$ | $\rho_{\text{core}} / 10^{-6} \text{ \AA}^{-2}$ | $\rho_{\text{shell}} / 10^{-6} \text{ \AA}^{-2}$ | $Z$  |
|---------------------|-----------------|-----------------|-----------------|-----------------------|-------|---|--|------|
| 0.75                | 2.39            | 1.09            | 1.35            | 3.74                  | 2.2   | 8.58  | 9.67   | 19.0 |
| 0.50                | 2.42            | 1.02            | 1.38            | 3.80                  | 2.4   | 8.04  | 9.72   | 18.7 |
| 0.25                | 2.51            | 1.02            | 1.40            | 3.91                  | 2.4   | 7.70  | 9.69   | 18.8 |

**Figure 8.** SAXS patterns measured for [surfactant] = 15 mmol L<sup>-1</sup>, 0.2% m/v PEI and different  $\chi_{\text{NaC}}$  according to the legend.

Considering that the first methylene units of the surfactant chains makes part of the polar region, the hydrophobic core of the micellar aggregates comprises the C<sub>11</sub>H<sub>23</sub> fragment of the linear SDS chains and the C<sub>22</sub>H<sub>37</sub>O<sub>3</sub> fragment of NaC. Since the scattering length density is proportional to  $\sum n_i z_i$  (which is the number of electrons of each apolar segment), C<sub>22</sub>H<sub>37</sub>O<sub>3</sub> has approximately two times more electrons than the apolar region of SDS, C<sub>11</sub>H<sub>23</sub> (89 e<sup>-</sup> for SDS and 193 e<sup>-</sup> for NaC). Therefore, it is clear that when  $\chi_{\text{NaC}}$  increases,  $\rho_{\text{core}}$  increases (Table 3) and approaches  $\rho_{\text{water}}$  ( $9.42 \times 10^{-6} \text{ \AA}^{-2}$ ). Thus, the scattering length density contrast of the core ( $\rho_{\text{core}} - \rho_{\text{water}}$ ), which is the main contributor to the  $P(q)$  signal, is reduced making difficult (if not impossible) to observe the micellar form factor. This happens due to an inadequate particle-solvent contrast. The reduction in the number of aggregation as  $\chi_{\text{NaC}}$  increases (not shown here) also contributes to the reduction in the bump region signal.

To summarize, the aggregate size and shape are only slightly dependent on  $\chi_{\text{NaC}}$ , although great differences in the SAXS profiles are observed. Besides, the sharp interference peak in the low- $q$  region does not show any systematic trend as a function of  $\chi_{\text{NaC}}$ , remaining basically in the same position and with approximately the same intensity.

## Conclusions

The association of the bile salt sodium cholate (NaC), sodium dodecyl sulfate (SDS) and mixtures of these two

surfactants with the polyelectrolyte poly(ethyleneimine) (PEI) was investigated in detail by means of pH value, electrical conductivity, steady-state fluorescence and SAXS measurements. The fluorescence, pH and conductivity results suggested that the polyelectrolyte-surfactant association takes place through two steps: (i) the NaC and SDS entities bind specifically to sites of the PEI chains via electrostatic interaction and (ii) a self-assembly through regular cooperative association and hydrophobic interactions occurs. The NaC-PEI interaction is weaker; however, it can be enhanced by adding SDS to the NaC-PEI system leading to the formation of mixed NaC-SDS micelles which more strongly interact with the polyelectrolyte PEI, as evidenced by the fluorescence measurements and also determination of  $\Delta G^o$  as a function of  $\chi_{\text{NaC}}$ . The SAXS results suggested an ellipsoidal characteristic and micelles aggregates independently of the surfactant concentration or  $\chi_{\text{NaC}}$ . The supramolecular entities are smaller at higher surfactant concentrations and their size and shape are only slightly dependent on  $\chi_{\text{NaC}}$ . The SAXS fitting procedures also evidenced changes in the scattering length density contrast of the hydrophobic core as a function of  $\chi_{\text{NaC}}$  which also supports the formation of NaC-SDS mixed micelles.

## Acknowledgements

We acknowledge the Brazilian Synchrotron Light Laboratory (LNLS, Campinas-SP, Brazil) for the beamline use and Conselho Nacional de Desenvolvimento Científico e Tecnológico (CNPq) for the financial support and PhD fellowships. F. C. G. acknowledges Fundação de Amparo à Pesquisa do Estado de São Paulo (FAPESP) (grant No. 2010/06348-0).

## References

1. Small, D. M.; Penkett, S. A.; Chapman, D.; *Biochim. Biophys. Acta* **1969**, *176*, 178.
2. Barry, B. W.; Gray, G. M. T.; *J. Colloid Interface Sci.* **1975**, *52*, 314.
3. Oakenfull, D. G.; Fisher, L. R.; *J. Phys. Chem.* **1977**, *81*, 1838.
4. Fisher, L. R.; Oakenfull, D. G.; *J. Phys. Chem.* **1980**, *84*, 936.
5. Zana, R.; Guveli, D.; *J. Phys. Chem.* **1985**, *89*, 1687.
6. Kratochvil, J. P.; Hsu, W. P.; Kwok, D. I.; *Langmuir* **1986**, *2*, 256.

7. Small, D. M.; *Adv. Chem. Series* **1968**, 84, 31.
8. Coello, A.; Meijide, F.; Nunez, E. R.; Tato, J. V.; *J. Phys. Chem.* **1993**, 97, 10186.
9. Ju, C.; Bohne, C.; *J. Phys. Chem.* **1996**, 100, 3847.
10. Waissbluth, O. L.; Morales, M. C.; Bohne, C.; *Photochem. Photobiol.* **2006**, 82, 1030.
11. Partay, L. B.; Jedlovsky, P.; Segal, M.; *J. Phys. Chem. B* **2007**, 111, 9886.
12. Partay, L. B.; Segal, M.; Jedlovsky, P.; *Langmuir* **2007**, 23, 12322.
13. Warren, D. B.; Chalmers, D. K.; Hutchison, K.; Dang, W. B.; Pouton, C. W.; *Colloids Surf., A* **2006**, 280, 182.
14. Meszaros, R.; Varga, I.; Gilanyi, T.; *Langmuir* **2004**, 20, 5026.
15. Nam, Y. S.; Kang, H. S.; Park, J. Y.; Park, T. G.; Han, S. H.; Chang, I. S.; *Biomaterials* **2003**, 24, 2053.
16. Shuai, X. T.; Merdan, T.; Unger, F.; Kissel, T.; *Bioconjugate Chem.* **2005**, 16, 322.
17. Goddard, E. D.; *J. Colloid Interface Sci.* **2002**, 256, 228.
18. Zanette, D.; Lima, C. F.; Ruzza, A. A.; Belarmino, A. T. N.; Santos, S. D.; Frescura, V. L. A.; Marconi, D. M. O.; Froehner, S. J.; *Colloids Surf., A* **1999**, 147, 89.
19. Holmberg, K.; Jonsson, B.; Kronberg, B.; Lindman, B.; *Surfactants and Polymers in Aqueous Solution*, John Wiley & Sons Ltda: Chichester, 2002.
20. Minatti, E.; Borsali, R.; Putaux, J. L.; Schappacher, M.; Deffieux, A.; Viville, P.; Lazzaroni, R.; Narayanan, T.; *Langmuir* **2003**, 19, 6.
21. Minatti, E.; Viville, P.; Borsali, R.; Schappacher, M.; Deffieux, A.; Lazzaroni, R.; *Macromolecules* **2003**, 36, 4125.
22. Zanette, D.; Ruzza, A. A.; Froehner, S. J.; Minatti, E.; *Colloids Surf., A* **1996**, 108, 91.
23. Minatti, E.; Zanette, D.; *Colloids Surf., A* **1996**, 113, 237.
24. Norwood, D. P.; Minatti, E.; Reed, W. F.; *Macromolecules* **1998**, 31, 2957.
25. Minatti, E.; Norwood, D. P.; Reed, W. F.; *Macromolecules* **1998**, 31, 2966.
26. Dal Bo, A.; Schweitzer, B.; Felipe, A. C.; Zanette, D.; Lindman, B.; *Colloids Surf., A* **2005**, 256, 171.
27. Schweitzer, B.; Felipe, A. C.; Dal Bo, A.; Minatti, E.; Zanette, D.; Lopes, A.; *J. Colloid Interface Sci.* **2006**, 298, 457.
28. Schweitzer, B.; Felipe, A. C.; Dal Bo, A.; Minatti, E.; Zanette, D.; *Macromol. Symp.* **2005**, 229, 208.
29. Zanette, D.; Felipe, A. C.; Schweitzer, B.; Dal Bo, A.; Lopes, A.; *Colloids Surf., A* **2006**, 279, 87.
30. Felipe, A. C.; Schweitzer, B.; Dal Bo, A. G.; Eising, R.; Minatti, E.; Zanette, D.; *Colloids Surf., A* **2007**, 294, 247.
31. Winnik, M. A.; Bystryak, S. M.; Chassenieux, C.; Strashko, V.; Macdonald, P. M.; Siddiqui, J.; *Langmuir* **2000**, 16, 4495.
32. Wang, H.; Wang, Y. L.; Yan, H.; Zhang, J.; Thomas, R. K.; *Langmuir* **2006**, 22, 1526.
33. Winnik, M. A.; Bystryak, S. M.; Siddiqui, J.; *Macromolecules* **1999**, 32, 624.
34. Bystryak, S. M.; Winnik, M. A.; Siddiqui, J.; *Langmuir* **1999**, 15, 3748.
35. Meszaros, R.; Thompson, L.; Bos, M.; Varga, I.; Gilanyi, T.; *Langmuir* **2003**, 19, 609.
36. Bastardo, L. A.; Garamus, V. M.; Bergström, M.; Claesson, P. M.; *J. Phys. Chem. B* **2004**, 109, 167.
37. Turro, N. J.; Yekta, A.; *J. Am. Chem. Soc.* **1978**, 100, 5951.
38. Turro, N. J.; Baretz, B. H.; Kuo, P. L.; *Macromolecules* **1984**, 17, 1321.
39. Zana, R.; Yiv, S.; Strazielle, C.; Lianos, P.; *J. Colloid Interface Sci.* **1981**, 80, 208.
40. Zana, R.; *Mixed Surfactant Solutions*, Marcel Dekker: New York, 1993, chapter 12.
41. Winnik, F. M.; Regismond, S. T. A.; *Colloids Surf., A* **1996**, 118, 1.
42. Cavalcanti, L. P.; Torriani, I. L.; Plivelic, T. S.; Oliveira, C. L. P.; Kellermann, G.; Neuenschwander, R.; *Rev. Sci. Instrum.* **2004**, 75, 4541.
43. Hammersley, A. P.; *Scientific Software FIT2D*, ESRF Synchrotron, France, 2009.
44. Hayter, J. B.; Penfold, J.; *Mol. Phys.* **1981**, 42, 109.
45. Kohlbrecher, J.; *Software Package SASfit for Fitting Small-Angle Scattering Curves*, Paul Scherrer Institute, Switzerland, 2010.
46. Jones, M. N.; *J. Colloid Interface Sci.* **1967**, 23, 36.
47. Schwuger, M. J.; *J. Colloid Interface Sci.* **1973**, 43, 491.
48. Benraou, M.; Bales, B.; Zana, R.; *J. Colloid Interface Sci.* **2003**, 267, 519.
49. Ghoreishi, S. M.; Li, Y.; Bloor, D. M.; Warr, J.; Wyn-Jones, E.; *Langmuir* **1999**, 15, 4380.
50. Zanette, D.; Ruzza, A. A.; Belarmino, A. T. N.; Santos, S.; Lima, C. F.; Froehner, S. J.; Frescura, V. L. A.; *J. Am. Chem. Soc.* **1997**, 213, 265.
51. Zanette, D.; Frescura, V. L. A.; *J. Colloid Interface Sci.* **1999**, 213, 379.
52. Lindman, B.; Wennerström, H.; *Top. Curr. Chem.* **1980**, 87, 1.
53. Caetano, W.; Gelamo, E. L.; Tabak, M.; Itri, R.; *J. Colloid Interface Sci.* **2002**, 248, 149.
54. Romani, A. P.; Gehlen, M. H.; Itri, R.; *Langmuir* **2005**, 21, 127.
55. Zemb, T.; Charpin, P.; *J. Phys. France* **1985**, 46, 249.
56. Colafemmina, G.; Fiorentino, D.; Ceglie, A.; Carretti, E.; Fratini, E.; Dei, L.; Baglioni, P.; Palazzo, G.; *J. Phys. Chem. B* **2007**, 111, 7184.
57. Santiago, P. S.; Neto, D. D. S.; Barbosa, L. R. S.; Itri, R.; Tabak, M.; *J. Colloid Interface Sci.* **2007**, 316, 730.
58. Tanford, C.; *J. Phys. Chem.* **1972**, 76, 3020.

Submitted: November 29, 2010  
Published online: May 10, 2011